NUCLEAR DATA AND MEASUREMENTS SERIES

ANL/NDM-157

FAST-NEUTRONS INCIDENT ON GADOLINIUM

by

Alan B. Smith

July, 2004

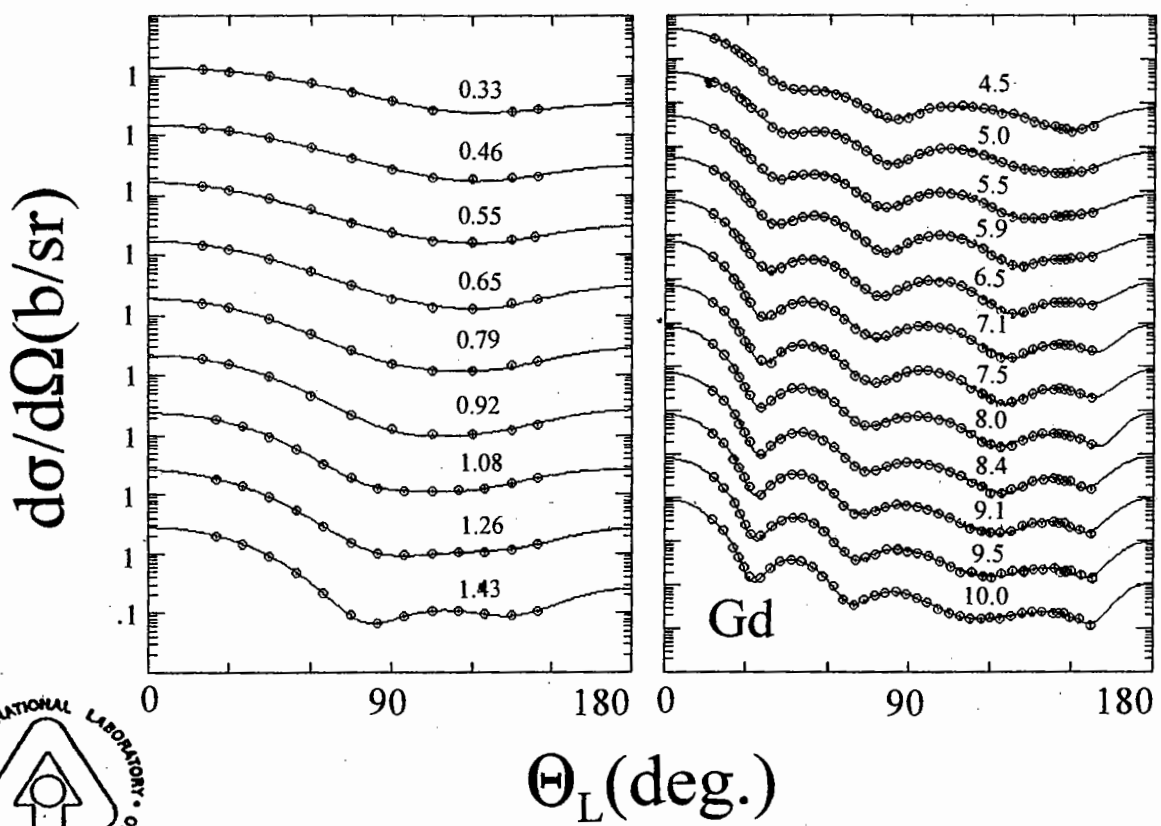

ARGONNE NATIONAL LABORATORY, ARGONNE, ILLINOIS

Operated by THE UNIVERSITY OF CHICAGO

for the U. S. DEPARTMENT OF ENERGY

under Contract W-31-109-Eng-38

Argonne National Laboratory, a U.S. Department of Energy Office of Science laboratory, is operated by The University of Chicago under contract W-31-109-Eng-38.

DISCLAIMER

This report was prepared as an account of work sponsored by an agency of the United States Government. Neither the United States Government nor any agency thereof, nor The University of Chicago, nor any of their employees or officers, makes any warranty, express or implied, or assumes any legal liability or responsibility for the accuracy, completeness, or usefulness of any information, apparatus, product, or process disclosed, or represents that its use would not infringe privately owned rights. Reference herein to any specific commercial product, process, or service by trade name, trademark, manufacturer, or otherwise, does not necessarily constitute or imply its endorsement, recommendation, or favoring by the United States Government or any agency thereof. The views and opinions of document authors expressed herein do not necessarily state or reflect those of the United States Government or any agency thereof.

Available electronically at http://www.osti.gov/bridge/

Available for a processing fee to U.S. Department of Energy and its contractors, in paper, from:

U.S. Department of Energy
Office of Scientific and Technical Information
P.O. Box 62
Oak Ridge, TN 37831-0062
phone: (865) 576-8401
fax: (865) 576-5728
email: reports@adonis.osti.gov

Nuclear Data and Measurement Series

Reports in the Argonne National Laboratory Nuclear Data and Measurement Series present results of studies in the field of microscopic nuclear data. The primary objective of the series is the dissemination of information in the comprehensive form required for nuclear technology applications. This Series is devoted to: a) measured microscopic nuclear parameters, b) experimental techniques and facilities employed in measurements, c) the analysis, correlation and interpretation of nuclear data, and d) the compilation and evaluation of nuclear data. Contributions to this Series are reviewed to assure technical competence and, unless otherwise stated, the contents can be formally referenced. This Series does not supplant formal journal publication, but it does provide the more extensive information required for technological applications (e.g., tabulated numerical data) in a timely manner.

Publications in the ANL/NDM Series

A listing of recent issues in this series is given below. Issues and/or titles prior to ANL/NDM-135 can be obtained from the National Technical Information Service, U. S. Department of Commerce, Technology Administration, Springfield, VA 22161, or by contacting the author of this report at the Nuclear Engineering Division, Argonne National Laboratory, 9700 South Cass Avenue, Argonne, IL 60439 (USA). In addition, the entire report series can be found on the Internet at the following URL: <http://www.td.anl.gov/reports/ANLNDMReports.html>, including abstracts, complete reports, and associated computer programs.

A. B. Smith and S. Chiba
Neutron scattering from Uranium and Thorium
ANL/NDM-135, February 1995

A. B. Smith
Neutron scattering and models:- Iron
ANL/NDM-136, August 1995

A. B. Smith
Neutron scattering and models:- Silver
ANL/NDM-137, July 1996

A. B. Smith and D. Schmidt
Neutron scattering and models:- Chromium
ANL/NDM-138 June 1996

W. P. Poenitz and S. E. Aumeier
The simultaneous evaluation of the standards and other cross sections of importance for technology
ANL/NDM-139, September 1997

D. L. Smith and J. T. Daly
A compilation of information on the ^{31}P(p,gamma)^{32}S reaction and properties of excited levels in ^{32}S
ANL/NDM-140, November 2000

A. B. Smith
Neutron scattering and models:- Titanium
ANL/NDM-141, July 1997

A. B. Smith
Neutron scattering and models:- Molybdenum
ANL/NDM-142, July 1999

R. E. Miller and D. L. Smith
Compilation of information on the ^{31}P(p,gamma)^{33}Cl reaction and properties of excited levels in ^{33}Cl
ANL/NDM-143, July 1997

R. E. Miller and D. L. Smith
A compilation of information on the $^{31}P(p,gamma)^{28}Si$ reaction and properties of the excited levels in ^{28}Si
ANL/NDM-144, November 1997

R. D. Lawson and A. B. Smith
ABAREX, a neutron spherical optical-statistical model code:- A user's manual
ANL/NDM-145, June 1999

R. T. Klann and W. P. Poenitz
Non-destructive assay of EBR-II blanket elements using resonance transmission analysis
ANL/NDM-146, 1998

A. B. Smith
ELEMENTAL-ABAREX:- A user's manual
ANL/NDM-147, June 1999

D. G. Naberejnev and D. L. Smith
A method to construct covariance files in ENDF/B formats for critical safety applications
ANL/NDM-148, June 1999

A. B. Smith
Neutrons and Antimony:- physical measurements and interpretations
ANL/NDM-149, July 2000

A. B. Smith and A. Fessler
Neutrons and Antimony:- neutronic evaluations of ^{121}Sb and ^{123}Sb
ANL/NDM-150, July 2000

A. B. Smith
Fast neutrons incident on Holmium
ANL/NDM-151, December 2000

R. D. Lawson and A. B. Smith
Technical note:- Dispersion contributions to neutron reactions
ANL/NDM-152, August 2001

A. B. Smith
Fast-neutrons incident on Hafnium
ANL/NDM-153, June 2001

D. L. Smith, Dimitri G. Naberejnev and L. A. Van Wormer
An approach for dealing with large errors
ANL/NDM-154, September 2001

A. B. Smith
Fast-neutron scattering from elemental Rhenium
ANL/NDM-155, August 2003

D. L. Smith
A demonstration of the lognormal distribution
ANL/NDM-156, July 2003

ANL/NDM-157

FAST-NEUTRONS INCIDENT ON GADOLINIUM*

by

Alan B. Smith
Argonne National Laboratory, Argonne, Illinois; and
The Physicist's Consultative, Ottawa, Illinois

July, 2004

Keywords:-
Measured neutron scattering from Gd at 0.3-1.5 MeV and 4.5-10 MeV. Optical-statistical and coupled-channels model analysis of experimental results. Basic and applied physical comments.

---

*This work supported by the United States Department of Energy under contract W-31-109-ENG-38.

TABLE OF CONTENTS

Abstract 7

I. Introduction 7

II. Experimental Procedures and Results 7

III. Physical Models

III-A. Optical-Statistical Models (SOM) 9

III-B. Coupled-Channels Rotational Models (ROTM) 12

III-C Dispersion Effects 14

IV. Some Comparisons with an Evaluation and Other Models 16

V. Concluding Remark 18

Acknowledgments 18

References 19

Appendices

1. Total Cross Section Measurements 20

2. Prior Elastic-Scattering Measurements 21

3. Prior Inelastic-Scattering Measurements 21

Tables 22

Figures 27

ANL/NDM-157

FAST-NEUTRONS INCIDENT ON GADOLINIUM

ABSTRACT

Results of measurements of neutron scattering from elemental gadolinium over the incident-energy regions of 0.3-1.5 MeV and 4.5-10.0 MeV are presented. These results are interpreted in terms of optical-statistical and coupled-channels models, including consideration of dispersion effects and of scalar and vector potentials. Some basic and applied physical implications of these considerations are noted. Comparisons are made with other regional models, and with ENDF/B-VI evaluated nuclear-data files used in applications.

I. INTRODUCTION

Elemental gadolinium consists of seven isotopes; ^{152}Gd (0.20%), ^{154}Gd (2.18%), ^{155}Gd (14.80%), ^{156}Gd (20.47%), ^{157}Gd (15.65%), ^{158}Gd (24.84%) and ^{160}Gd (21.86%). ^{155}Gd and ^{157}Gd are collectively-deformed even-odd rotors with a dense low-lying excited structure built upon the $3/2^-$ g.s. of the $3/2^-$[521] Nilsson orbital [(**MN59**), (**Pre62**)]. This level density far exceeds the resolutions of neutron-scattering measurements. The remaining isotopes (^{152}Gd, ^{154}Gd, ^{156}Gd, ^{158}Gd and ^{160}Gd) are even-even nuclei with protons in the $1g_{7/2}$ shell and neutrons in $2f_{7/2}$ and/or $1h_{9/2}$ shells. They are also collective rotors with the first-excited (2^+) state of the g.s. rotational band at ≈ 80 - 125 keV, the second-excited (4^+) state at ≈ 260 - 375 keV, and with the third-excited (6^+) state following at approximately twice the energy of the 4^+ state. The collective deformations are large, with $\beta_2 \approx 0.3$ and $\beta_4 \approx 0.05$ [(**NDS**), (**YA87**)]. .The experimental knowledge of the fast-neutron total and scattering cross sections of elemental and/or isotopic gadolinium is very limited and generally more than a quarter-century old, as outlined in Appendices **A-1, A-2** and **A-3**. The gadolinium isotopes are significant fission products and thus a concern in fission-energy systems. Further, they are in a region of collective deformation where there are a number of other fission products. Models for extrapolation and prediction of fast-neutron reactions in this mass region are of continuing basic and applied interest. The present work was undertaken to address some of these issues.

II. EXPERIMENTAL PROCEDURES AND RESULTS

Very early work at the Argonne National Laboratory resulted in gadolinium scattering data distributed between 0.3 and 1.5 MeV (**SSW70**). That work is now nearly forty years old. During the intervening years a number of additional measurements have been made at Argonne over the same incident-energy range. Reference **SSW70** reports 65 elastic-scattering distributions, and the subsequent measurements resulted in 31 additional elastic distributions.

The measurement methods of reference **SSW70** and those of the additional low-energy results reported here were essentially the same. All of the measurements employed the time-of-flight technique (**CL55**), concurrently using eight flight paths of approximately 2 m length distributed over a scattering angular range of ≈ 25° - 160° at each incident energy. The neutron source was the $^{7}Li(p,n)^{7}Be$ reaction (**Dro87**). The uncertainties of the measured differential "elastic"-scattering results were estimated to be <≈ 8%. The incident-neutron resolutions were ≈ 20 - 30 keV and the scattered-neutron resolutions were ≈ 50 keV below incident energies of ≈ 900 keV. From 0.9 - 1.5 MeV the scattered-neutron resolutions were somewhat uncertain, but estimated to be ≈ 100 keV. These resolutions imply that the measured results represent elastic scattering at incident energies of less than ≈ 900 keV, with the possible exception of modest contamination from the excitation of the first level of ^{157}Gd;. At higher incident energies there is possible contamination of the "elastic" results by inelastic scattering resulting in the excitation of the 2^{+} levels of the even-even isotopes, and from several of the low-lying levels of the even-odd isotopes. All of the low-energy measurements were made relative to the total scattering cross sections of C or Zr as reported by Lane et al. (**Lan+61**). The new low-energy results were combined with the older data of reference **SSW70** and averaged over ≈ 150 keV incident-energy bins in order to smooth fluctuations and reduce the data base to manageable proportions for the subsequent interpretations. The resulting nine averaged distributions are shown in the left panel of **Figure II-1.** There were some associated lower-energy inelastic-scattering results which are discussed in **Sec. III-B**, below.

The second and higher-energy portion of the present measurements extend over the incident-neutron energy range 4.5 - 10.0 MeV with twelve approximately equal-energy-spaced "elastic" differential distributions. Each distribution consisted of ≈ 40 differential values distributed between ≈ 18^{0} and 160^{0}. The $^{2}D(d,n)^{3}He$ reaction (**Dro87**) was used as the neutron source at these higher incident energies. The scattered-neutron resolutions were ≈ 300 keV, Thus the inelastic scattering resulting from the excitation of the low-lying levels of the various gadolinium isotopes was not resolved from the elastic component. In particular, the measured values included neutrons due to the excitation of the first two excited levels of the even-even gadolinium isotopes with the elastically-scattered contribution. These higher-energy measurements also employed the time-of-flight technique, with the concurrent use of ten ≈ 5 m flight paths. The cross sections were measured relative to the H(n,p) scattering standard (**CSL83**). The estimated cross-section uncertainties associated with these higher-energy measurements varied from a minimum of 3% in regions of large cross section to >≈ 10% at the diffraction minima. These higher-energy "elastic"-scattering results are illustrated in the right panel of **Figure II-1**

All of the present measurements used cylindrical samples of high-purity elemental metallic gadolinium, approximately 2.0 cm in diameter and 2.0 cm long. All of the experimental results were corrected for angular-resolution, beam attenuation and multiple-event effects using Monte-Carlo procedures (**Smi90**). Various versions of the time-of-flight system used in the above measurements operated at The Argonne National Laboratory for over thirty years. They are extensively described elsewhere (**Smi92**).

III. PHYSICAL MODELS

III-A. OPTICAL-STATISTICAL MODELS (SOM)

The initial physical considerations were based upon the spherical, weak-coupling, optical-statistical model (SOM) [(**Wol51**), (**Fes58**)]. Above a few keV gadolinium compound-nucleus resonances grossly overlap, resulting in slowly-varying energy-dependent cross sections. Such energy-average cross sections are consistent with the present experimental results and the concepts of the SOM . As outlined in Appendixes **A-2** and **A-3**, the present experimental data, and the early work by the author and coworkers (**SSW70**), constitute the very large majority of the experimental gadolinium scattering data available for physical interpretation or applications use. Even these resources are meager, only extending over ≈ 0.3 - 1.5 and 4.5 - 10.0 MeV incident-energy regions. There is very little in the energy range between, and nothing at higher energies. Throughout this work, all the model potentials were assumed to consist of a Saxon-Woods real form, a Saxon-Woods-Derivative imaginary form and a real Thomas spin-orbit form (**Hod63**). The spin-orbit parameters were taken from reference **WG86**. Direct and compound-nucleus processes were given explicit attention. In doing so, the first eight discrete levels of each of the seven isotopes of elemental gadolinium were considered, with the energies, spins and parities as given in the Nuclear Data Sheets (**NDS**). The excitation of higher-lying levels was treated statistically using the concepts and parameters of Gilbert and Cameron (**GC65**). Thus, the discrete level representations for the even-even isotopes extended to an MeV or more, but only to several-hundred keV for the two odd isotopes. The calculations included resonance width fluctuation and correlation corrections in the manner of Moldauer (**Mol80**). Compound-nucleus processes were considered only as relevant to neutron scattering. This is not a limitation in these gadolinium interpretations. Radiative capture above a few keV is relatively small and can reasonably be ignored. Charged-particle-emission processes are small below the 10 MeV upper energy limit of the measurements and thus similarly were ignored. The (n,2n) reactions are small below 8 - 9 MeV, but then rise rapidly with increasing energy, and may approach several barns at 10 - 12 MeV. Ignoring them may distort the interpretation of the scattering cross sections at the extreme upper-energy limit of the present scattering data. The elemental SOM calculations were carried out using the code ELEMENTAL ABAREX (**Smi99**). This program concurrently treats the structure of the individual isotopes, combines the calculated isotopic components to obtain the model elemental value and then compares it with the elemental observables. In doing so, real and imaginary iso-vector contributions are considered. This code also has an option for the introduction of additional exit channels, such as fission or (n,2n) processes, but this option was not used here.

The SOM parameters were obtained by explicitly Chi-square fitting neutron total and differential "elastic"-scattering cross sections. The fitting followed through six sequential steps. First, the six real and imaginary potential parameters were varied from which the real-potential diffuseness (a_V) was fixed. Then followed five steps progressively fixing the real reduced radius (r_V, where $R_i = r_i \cdot A^{1/3}$), the imaginary reduced radius (r_W), the imaginary

diffuseness (a_W), the real-potential strength (V), and the imaginary-potential strength (W). The entire procedure was repeated three times in an iterative manner. The data base included all the "elastic" scattering data of **Figure II-1** and energy-averaged total cross sections at the same energies taken from the data base of Appendix **A-1**. Inelastic-scattering data was not used in the fitting due to uncertain knowledge of the contributing level structure. The uncertainties assigned to the scattering data in the fitting procedures were taken from the measured values, as outlined in **Sec. II**. The total cross sections were given additional weight equivalent to that of three differential values in order to assure some effect in the fitting procedures. The experimental resolutions were considered, isotope by isotope, combining calculated inelastic and elastic scattering so as to be consistent with the experimental resolutions. These combinations differed depending upon the respective isotopic excited structure, the estimated experimental resolutions and the incident neutron energies. .

Basic concepts of nuclear forces and experimental observation [**(Lan62)**,**(GPT68)**, **(Sat69)**, **(Hod94)**, **(BG69)**] suggest an iso-spin dependence of the SOM. It is manifest by real and imaginary SOM (and coupled-channels model) potentials having the forms:-

$$V = V_0 \mp V_1 \cdot \eta$$

and **(III-A-1)**

$$W = W_0 \mp W_1 \cdot \eta,$$

where V_0 (W_0) is the "scalar" value and V_1(W_1) is the "vector" value, $\eta = (N-Z)/A$ is the target asymmetry, and the signs are "-" for neutron-induced and "+" for proton induced processes. This asymmetry effect is a manifestation of the iso-spin dependence of the potential, as discussed in the references. The value of η varies from 0.158 to 0.200 across the gadolinium isotopes. Therefore, one might expect a sensitivity to asymmetry in the present considerations. ELEMENTAL ABAREX utilizes scalar and vector potentials. The literature indicates that V_1 is twice the magnitude of W_1, and values applicable to the gadolinium mass region are reported to be V_1 = 16 Mev and W_1 = 8 MeV (**YA87**). In other mass regions values of 24 and 12 Mev, respectively, are frequently employed. The vector strengths are not well defined as the necessary experimental isotopic neutron, (p,p) and (p,n) results are not generally available. That is true in this work as the scattering sample is elemental gadolinium. With the lack of firm experimental evidence for gadolinium, the regional values of V_1 = 16 Mev and W_1 = 8 Mev were used in the primary SOM calculations. The above fitting procedures resulted in the SOM parameters given in **Table-A-1**. The entire elemental SOM fitting procedures were repeated assuming the alternate values V_1 = 24 Mev and W_1 = 12 Mev. There appeared to be no significant change in the results, although of course the numerical values of the scalar-potential strengths did change.

The above SOM is only a first approximation to the fast-neutron interaction with highly deformed collective rotators, such as the gadolinium isotopes. However, it may have some practical usefulness; e.g. for predicting low-energy radiative capture or as a starting point for DWBA calculations. The SOM calculations qualitatively describe what is known of the neutron total cross sections to at least 20 MeV, as illustrated in the upper panel of **Figure III-A-1**. The

only significant discrepancies between measurement and calculation are in the ≈ 1.5 - 4.5 MeV region where no reliable scattering data is available for SOM derivation. The SOM gives a reasonably good description of the observed "elastic"-neutron-scattering distributions, as illustrated in **Figure III-A-2**. Discrepancies between measurement and calculation shown in that figure are primarily in regions where the experimental resolutions are uncertain, or in the minima of the higher-energy distributions where the observables contain appreciable inelastic-scattering contributions which are largely due to direct excitations of the g.s. rotational bands, a mechanism that is inconsistent with the SOM. The SOM real-potential radius is quite small, while the associated imaginary radius is large, together with a small imaginary diffuseness (see **Table III-A-1**).. Such trends tend to be characteristic of SOM representations of the neutron interaction with highly deformed collective rotors in this mass-energy range. The effects are confused by the well-known correlations between real-potential depth and radius, and between imaginary-potential depth and diffuseness. The SOM real strength, represented as a volume-integral-per-nucleon (J_V), is unusually small while that for the imaginary potential (J_W) is larger than for the ROTM, below. S_0 and S_1 strength functions of ^{158}Gd calculated with the SOM are 1.35 and 2.85, compared to the respective values of 1.6 ∓ 0.2 and 1.3 ∓ 0.4 deduced from resonance measurements (**MDH81**). The agreement is qualitatively reasonable, remembering that ^{158}Gd is in a mass region where strength functions are considerably distorted by collective deformations.

The above is an elemental interpretation. A simpler approach based on a single-isotope approximation may be more useful in some cases. Furthermore, the author does not know of another SOM code, or a coupled-channels code, capable of handling multi-isotopic elemental fitting calculations in a manner analogous to that of ELEMENTAL ABACUS. Thus an isotopic approximation is necessary for the coupled-channel interpretations discussed in **Sec. III-B**, below. In view of these considerations a SOM model based on a single-isotope approximation was derived. That model assumed the target mass and excited structure of ^{158}Gd (i.e. the ^{158}Gd of the elemental calculational input). With this simplified SOM the entire fitting procedure described above was repeated with the resulting potential parameters of **Table III-A-2**. They are reasonably consistent with those of the full elemental potential of **Table III-A-1**, bearing in mind that **Table III-A-1** presents scalar strengths and **Table III-A--2** full potential strengths. In view of this consistency, it is not surprising that the two SOM representations result in gadolinium elemental total cross sections that are in good agreement, as illustrated in **Figure III-A-1**. The differential "elastic" scattering calculated with the two SOM potentials is also in very close agreement, as evidenced by comparing **Figures III-A-2** and **III-A-3**. This suggests that, when dealing with the SOM of elemental gadolinium neutron "elastic"-scattering and total cross sections, either of the above potentials can be reasonably used. This conclusion supports the following coupled-channels interpretation where a mono-isotopic gadolinium "element" is used to approximate the complex natural isotopic structures.

III-B. COUPLED-CHANNELS ROTATIONAL MODELS (ROTM)

All of the isotopes of gadolinium are strong collective rotors with β_2 values of approximate 0.28 - 0.30 and β_4 values of 0.065 - 0.043 [(**NDS**), (**YA87**)]. Thus direct excitation of the collective levels of the ground-state (and higher) rotational bands of each isotope should be expected, with a sharp impact on the predicted fast-neutron-scattering cross sections and the associated model derivations. Such effects are inconsistent with the above SOM interpretations. A vehicle for interpreting these direct processes is the rotational coupled-channels model (ROTM), described by Tamura (**Tam65**) and by Raynal (**Ray93**). An application of that model to the present case is complicated by the multi-isotopic nature of the element, the combination of even-even and even-odd isotopes and the unavailability of a coupled-channels calculational vehicle that will fit elemental data with concurrent consideration of the various isotopic components of the element (as per the ELEMENTAL ABACUS used above in the above SOM context). With these obstacles the elemental experimental interpretation must be based upon an isotopic approximation of the element. The above SOM considerations suggest that such an approach should give reasonably quantitative results, and thus it was used in the present coupled-channels rotational model. Of the seven gadolinium isotopes, ^{152}Gd was abandoned as being of too small an abundance (0.2%) to have any influence in the present considerations. The β_2 and β_4 values of the remaining six gadolinium isotopes [(**NDS**), (**YA87**)] were averaged, weighting with the respective isotopic abundances. The resulting average values, used in the present ROTM, were $\beta_2 = 0.308$ and $\beta_4 = 0.056$. The target mass was taken to be the elemental mass (157.25 AMU). The excited structure of the assumed rotation target presents a problem as 30.45% of the element consists of the two even-odd isotopes, ^{155}Gd and ^{157}Gd. They are both collective rotors but each has a profusion of low-lying excited states. It was assumed that the cumulative effect of these many levels of the two even-odd isotopes would be reasonably represented by the 2+ and 4+ sequence of the first two excited states of the most prominent even-even isotope, ^{158}Gd. The levels of that isotope were also assumed to represent the discrete levels of the other even-even isotopes. The statistical continuum was taken to be that of ^{158}Gd, again using the parameters and representation of reference (**GC65**). Thus the ROTM was essentially based upon the isotope ^{158}Gd.

With the above isotopic approximation, the differential scattering data was fitted, using the code ECIS96 (**Ray96**), to obtain ROTM model parameters. In doing so the same eight discrete levels and the continuum of levels employed in the SOM fitting were used. The physical treatment of the compound-nucleus processes was analogous to that of the SOM. Furthermore, as in the SOM case, the calculations were arranged so as to be consistent with the experimental resolutions, assuming that the observed scattering distributions correspond to elastic processes up to incident energies of 1.0 MeV, to elastic plus first-inelastic group from the g.s. rotational band for incident energies of 1.0 to 1.5 MeV, and to elastic plus first and second inelastic groups from the g.s. rotational band at incident energies above 1.5 Mev. A number of fits were made using the entire scattering data base of **Figure II-1**, and parts thereof. The total cross sections were not an explicit part of the fitting procedure, as in the SOM case, but comparisons of measured and calculated total cross sections were made using various ROTM results. The

ROTM fitting initially followed the six-step sequence, outlined above in the context of the SOM, through several iterations. The parameter scatter was significant, particularly that of the imaginary diffuseness.. However, after a number of attempts it became evident that the potential geometries were essentially the same as the gadolinium values of Young and Arthur (**YA87**), thus their geometries were accepted for subsequent ROTM fitting, varying only real and imaginary strengths. The resulting ROTM potential parameters are given in **Table III-B-1**. This potential gave a very good description of the elemental neutron total cross sections, as shown in **Figure III-B-1.** The difference between measured and calculated values is generally within experimental uncertainty from a few keV to nearly 20 MeV, even though the measured values display some small energy-dependent fluctuations that are not consistent with the underlying concepts of the SOM or ROTM. The potential of **Table III-B-1** also gives a good description of the measured elemental differential-scattering cross sections , as illustrated in **Figure III-B-2.** This figure clearly shows the large differences between the simple elastic scattering and the observed differential values which are composites of elastic and inelastic contributions. Below incident energies of approximately ≈ 1.0 MeV the measurements are believed to resolve the elastic component from inelastic contributions, and the ROTM assumed that resolution. From 1.0 - 1.5 Mev the experimental resolution of the scattering is uncertain, particularly with respect to contributions from the odd isotopes. The figure suggests that, in the energy range 1.0 - 1.5 MeV, the resolution deteriorates, resulting in measured "elastic" values containing appreciable inelastic contributions. Above four MeV the measured differential values clearly contain elastic contributions together with the inelastic contributions from the excitation of the first two rotational levels of the assumed even-even target. This is consistent with the estimated experimental resolutions and the resolutions assumed in the use of the ROTM.

Figure III-B-2 gives emphases to the impact of inelastic scattering on the observed interaction of fast neutrons with the collective rotors of the gadolinium isotopes. The measurements were analyzed assuming that the first two inelastically-scattered neutron groups were due to the excitation of the 2^+ and 4^+ members of the g.s. rotational band of the even-even isotopes, composing approximately 2/3 of the elemental abundance. The remaining 1/3 of the abundance is approximately evenly split between the two even-odd isotopes ^{155}Gd and ^{157}Gd, both of which have a profuse low-energy collective structure. The experimental measurements approximated the low-excitation inelastic scattering with two neutron groups, corresponding to excitations of 80 and 260 keV, approximately the mean excitation energies of the 2^+ and 4^+ levels of the g.s. rotational band of the even-even isotopes. The same approach was used in references. **(SSW70)** and **(Tan+72).** The only other measurements attempting to describe discrete low-energy neutron inelastic scattering from isotopic and/or elemental gadolinium construe the process from (n,n';gamma) measurements. The latter provide good energy resolution but deduction of the underlying neutron cross sections is not straight forward. The present measurements resulted in approximately 30 cross section values relevant to the excitation of these two apparent levels. These were added to the earlier results of reference **(SSW70)** and the combined total averaged over 100 keV incident-energy increments. The results are shown in **Figure III-B-3,** together with the corresponding higher-energy results of Tanaka et al.(**Tan+72**). . The two sets of experimental results are reasonably consistent. **Figure**

III-B-3 also shows the corresponding results calculated with the ROTM potential of **Table III-2**. The agreement between measurement and calculation is remarkably good in view of the approximations involved. The inelastic scattering cross sections are large and, of course, consistent with the large differences shown in the calculated scattering angular distributions of **Figure III-B-2.** Perhaps the agreement between measurement and calculation, shown in **Figure III-B-3,** could be improved by somewhat reducing the β_2 value used in the calculations. However, such an adjustment is probably not warranted in view of the other approximations involved in both measurements and calculations.

III-C. DISPERSION EFFECTS

It is well known that there is a dispersion relationship coupling real and imaginary potentials and reflecting causality [(**Lan62**), (**Sat83**), (**Lip66**), (**Pas67**), (**Fes58**)]. This relationship can be expressed in the form

$$J_V(E) = J_{HF}(E) + (P/\pi)\cdot\int [\, J_w(E')/(E - E')]\cdot dE' \qquad \textbf{III-C-1}$$

where J_V is the strength of the real potential, J_{HF} that of the local-equivalent Hartree-Fock potential, and J_W the strength of the imaginary potential. "P" is the principle value of the integral which is evaluated from $-\infty$ to $+\infty$. Here, and throughout this section, strengths are give in the form of volume-integrals-per-nucleon unless otherwise stated. The above integral can be broken into surface, ΔJ_{sur}, and volume, ΔJ_{vol}, components

$$\Delta J_{sur}(E) = (P/\pi)\cdot\int [J_{sur}(E')/(E - E')]\cdot dE' \qquad \textbf{III-C-2}$$

and

$$\Delta J_{vol}(E) = (P/\pi)\cdot\int [J_{vol}(E')/(E - E')]\cdot dE'. \qquad \textbf{III-C-3}$$

Then $J_V(E) = J_{eff}(E) + \Delta J_{sur}(E)$ and $J_{eff}(E) = J_{HF}(E) + \Delta J_{vol}(E)$, where $J_{sur}(E)$ and $J_{vol}(E)$ are surface- and volume-imaginary potential strengths, respectively. J_{HF} and ΔJ_{vol} are both approximately linear functions of energy in the range of the present considerations, thus the individual components can not be experimentally resolved. The effect of **Eq. III-C-2** is to add a surface component to the real potential that is some fraction of the imaginary potential. The magnitude of this contribution was calculated using the methods of Lawson et al. (**LGS87**) and Lawson and Smith (**LS01**). The latter reference presents a detailed description of the theory and method, and includes a FORTRAN code for executing the calculations. In the present application it was assumed that ΔJ_{sur} retained the geometric parameters and Saxon-Woods-Derivative form of the imaginary potential, varying only in magnitude. This is an assumption that is not necessarily true, but there appears to be no guidance as to alternate shapes. The experimental data base and associated models are strictly relevant only to the energy range of 0 - 10 MeV. The above integrals extend from $-\infty$ to $+\infty$, thus approximations are required. It was assumed that the

imaginary potential was entirely a surface effect up to 10 MeV, and then the surface component fell linearly to zero at 80 MeV. Concurrently, a volume-imaginary potential was taken to rise linearly from zero at 10 MeV to 80 MeV where it took the J_{sur} 10 MeV magnitude, and then remained constant to infinity. Further, the imaginary potential was assumed to be zero at the Fermi energy (E_F) and to have a quadratic energy dependence from E_F to zero energy. The Fermi energy was taken to be -6.99 MeV as determined from the mass tables (**TUL90**). Throughout, the considerations, the entire imaginary potential was taken to be symmetric about the Fermi energy.

Following the above procedures, the ΔJ_{sur} of **Eq. III-C-2** was calculated from the ROTM potential of **Table III-B-1**. This calculation determines the contribution of the imaginary potential that must be reflected into the real potential as a function of incident energy due to dispersion effects. This fraction decreases from somewhat more than unity at zero energy to values smaller than unity at 20 MeV. The magnitudes and energy dependancies are somewhat dependent on the choice of the energy extrapolations cited above. The dispersion fraction was converted to the surface real-potential contribution. The entire ROTM fitting procedure, including the dispersion contribution, was repeated several times in an iterative manner, including re-determination of the dispersion contribution at each iteration. The resulting dispersion ROTM parameters are given in **Table III-C-1.** These parameters are consistent with those of **Table III-B-1**, considering the contribution of the dispersion contribution to the strengths. The dispersion ROTM gives an excellent description of the observed total cross sections, as illustrated in **Figure III-C-1**, and similar to that given by the ROTM. Which of the two potentials is better is arguable as the dispersion version gives somewhat better agreement with the measured total cross sections up to approximately 10 - 12 MeV but is somewhat less suitable at higher energies, The dispersion ROTM gives a very good representation of the observed differential "elastic" scattering, essentially identical to that obtained with the ROTM and illustrated in **Figure III-B-2**. Thus, while the dispersion effect is doubtless a physical reality, the experimental knowledge of neutron scattering from gadolinium is not sufficient to precisely define it.

The energy dependence of the ROTM real potential is small. It increases somewhat with the introduction of dispersion effects but still remains small. The real-potential energy dependence is related to the effective mass through the expression

$$m^*/m = 1 - (dV^L/dE) \qquad \textbf{(III-C-4)}$$

where m is the nucleon mass, m* the effective mass and V^L the local real potential. The ROTM values imply a m*/m ratio of approximately 0.9 rather than the 0.68 predicted by theoretical estimate [(**BDS79**), (**GPT68**), (**MN81**)], Furthermore, the magnitude of the energy dependence of the ROTM real potential is only about a third that implied from considerations of the non-locality of nuclear forces (**PB62**). The energy dependence of the real isotopic-gadolinium potentials of reference **YA87** are also smaller than the trend in this mass region, though not as acutely so as in the present work. The effect is also evident in the potential comparisons of

Table IV-1(A). The underlying reasons for this unusual energy dependence of the real potential remain unknown. However, it has been noted that low-energy neutron total cross sections in this mass region can differ by noticeable amounts, and this can be reflected in the energy dependence of the real potential.

IV. SOME COMPARISONS WITH AN EVALUATION AND WITH OTHER MODELS

There are several nuclear evaluated file systems distributed about the world. The United States System is the Evaluated Nuclear Data File/B, Version VI (ENDF/B-VI) [(**ENDF**), (**NNDC**)]. It is perhaps the first such evaluated-file system, and it is frequently updated. Many of the other evaluation systems use the same formats as ENDF/B, and frequently much of the same numerical content. ENDF/B-VI presents evaluations for all of the naturally occurring isotopes of gadolinium from which an elemental file can be constructed. However, there is no elemental gadolinium file. That is unfortunate as direct simple comparison with elemental measurements is not possible. All of the ENDF/B-VI gadolinium files are elderly, generally being modest upgrades of several previous versions. This is not a-priori bad as the experimental data base has been essentially dormant for decades. However, during the same period modeling capability for evaluation has generally advanced.

The ENDF/B elemental total cross sections, constructed from the isotopic files, are compared with the measured values in **Figure IV-1**. The agreement is remarkably good, possibly because the total cross sections of the files are largely based upon elemental experimental information which has not changed. Comparisons are not as favorable in the context of neutron elastic scattering, as illustrated by the examples of **Figure IV-2**. That figure compares ^{158}Gd evaluated differential elastic-scattering distributions with results obtained with the ROTM of the present work at representative energies. The large disagreements are not surprising as the evaluated elastic distributions seem to have been generated with an ancient spherical optical model. Such a model is not appropriated for representation of the neutron interaction with highly-deformed collective rotors, such as the gadolinium isotopes. **Figure IV-3** compares the ENDF/B-VI ^{158}Gd angle-integrated elastic-scattering cross sections with results of ROTM calculations (compound-elastic (CE), direct elastic (DIR) and total-elastic cross sections). The ENDF/B-VI elastic cross sections are said to be simply the difference between the total cross section and the sum of other partial cross sections. The results are sensitive to competition from the large (n,2n) cross section which has a threshold of ≈ 8 MeV. Both below and above this threshold the evaluation is inconsistent with the ROTM predictions. One can also angle-integrate the experimental "elastic" distributions using legendre-polynomial fitting to obtain "experimental" angle-integrated "elastic" cross sections. Remembering that these experimental values consist of elastic + the first-two-inelastic contributions above 4 MeV, and that the ENDF/B considerations are limited to compound-nucleus inelastic scattering, one finds that the ENDF/B-VI elastic scattering is much larger than implied by the experimental measurements. Clearly, the ENDF/B-VI gadolinium files are in need of review. This may be why macroscopic neutronic calculations frequently use empirical lumped fission-product files

rather than the ENDF/B-VI isotopic files. To the extent that other evaluated file systems use all or part of the ENDF/B-VI gadolinium files , the above remarks apply.

Over the last few years there have been a number of models of the fast-neutron interaction with rotational and vibrational collective targets in the mass region of gadolinium, largely as the result of work at Los Alamos and Argonne National Laboratories. One of these is that for the isotopes of gadolinium by Young and Arthur (**YA87**). That model is remarkably similar to the ROTM of the present work, as noted in **Sec. III-3**. So much so that the two models were taken to have identical geometry. The **YA87** model gives a very good description of the measured total cross sections, nearly as good as that of the ROTM. The **YA87** potential also provides a description of the present differential-scattering results very similar to that of the ROTM. The suitability of the model of reference **YA87** is more the remarkable as it was developed without the benefit of the present experimental results. A number of potential strengths in this mass region of collective deformation, are summarized in terms of volume-integrals- per- nucleon in **Table IV-1(A)**. Throughout the derivation of this table only results below 10 MeV were used. Volume absorption was ignored and all energy dependencies were approximated with linear expressions. The geometries of the various potentials vary but are not entirely independent. Thus it is important to make the comparisons in terms of volume-integrals-per-nucleon. The real-potential volume integrals are reasonably similar except for the energy dependence of the gadolinium potentials of the present work, and to a lesser extent of reference **YA87,** which is smaller than the average, as noted above. No systematic dependence of the real strengths of **Table IV-1(A)** on Z, A, η or β_2 was identified. The imaginary volume integrals are surprisingly consistent as the approximations used in their derivations had to deal with varying contributions from volume absorption, and non-linear energy dependence in one case. At low energies all of the imaginary strengths are quite small, and all rise with energy at approximately the same rapid rate. The representations of **Table IV-1(A)** are strictly valid to only 10 MeV. At higher energies one can no longer ignore volume absorption, and the imaginary strength can not increase indefinitely.

The above potential strengths and their energy dependencies can be averaged assuming an average target mass of 168.4 AMU and an average β_2 of 0.3. Similarly, the various geometric factors can be averaged though, as noted above, they are not always independent. From these averages a general "regional " potential is obtained, as cited in the lower portion of **Table IV-1 (B)**. This "regional potential" was used to calculate elemental gadolinium neutron total and scattering cross sections. The total-cross-section results are compared with the experimental values in **Figure IV-4** (upper panel). The agreement is very good above several MeV. At lower energies the calculated values tend to be a few percent larger than the experimental values. This difference is very sensitive to the zero-energy value of the real potential strength. If that value is lowered by only 1.0% a much better low-energy agreement is obtained from the calculations, as illustrated in the lower panel of **Figure IV-4**. The "regional" potential of **Table IV-1 (B)** was also used to calculate the differential "elastic"-scattering cross sections of elemental gadolinium with results which were very similar to those shown in **Figure III-B-2**.

The above comments suggest that the "regional" potential of **Table IV-1(B)** can provide quantitatively reasonable fast-neutron data for the collective rotational and/or vibrational nuclei in the A = 150 - 190 region using coupled-channels calculational concepts. Implementation of such an endeavor in a systematic manner has the potential for considerable improvement in evaluated file systems in an important fission-product region.

V. CONCLUDING REMARK

The experimental knowledge of fast-neutron interactions with gadolinium and/or its isotopes is poor. The present work is the first major contribution to such knowledge in more than thirty years. Even the neutron total cross sections are only marginally known, with no information above 20 MeV. Thus, it is not surprising that at least some of the contemporary evaluated gadolinium files are discrepant with the results of the present new measurements. As demonstrated in the above discussion, collective coupled-channels models based upon regional understanding of parameterizations can give a quantitatively reasonable description of many fast-neutron processes. Unfortunately, they have not been used in the gadolinium evaluations of ENDF/B. The result is evaluations of major fission products that are questionable. The techniques for providing the requisite experimental information are well known but the available facilities for such measurements are vanishing, together with the associated skilled personnel. The model-computational situation is somewhat better, but even there the skilled personnel and knowledge are fading. Furthermore, physics is an observational science and thus there is a limit to the computational extrapolation of measured observables. Comprehensive measurements will probably require isotopic research samples. It is not clear that the resources of such samples for measurements continues to exist. The applied gadolinium situation is not good for this major fission product. As in a number of other cases, the experimental knowledge of gadolinium (p,n) and (p,p) processes is largely nonexistent, or is lost in the mists of time. This makes it difficult or impossible to assess some of the fundamental physical properties, particularly those dealing with iso-spin.

ACKNOWLEDGMENTS

The author would like to thank Drs. J. Raynal, P. Young and F. Kondev for their technical advice. The author is also indebted to the National Nuclear Data Center, Brookhaven Natl. Lab. for the efficient provision of essential nuclear data, and to Mr. J. Bolling and associates for providing the computation facilities used in much of this work.

REFERENCES

(BG69) F. Becchetti Jr., and G. Greenlees, Phys. Rev. **182** 1190 (1969).

(BDS79) G. Brown, J. Dehesa and J. Speth, Nucl. Phys. **A330** 290 (1979).

(CL55) L. Cranberg and J. Levin, **Proc. Conf. on Peaceful Uses of Atomic Energy** Geneva, United Nations Press (1958).

(CSL83) **IAEA Tech. Report 227** (1983), Eds. H. Conde, A. Smith and A. Lorenz..

(Dro87) M. Drosg, IAEA Report **IAEA-TECDOC-410** (1987).

(ENDF/B) Evaluated Nuclear Data File/B-VI, National Nuclear Data Center, Brookhaven Natl. Lab.

(Fes58) H. Feshbach, Ann. Rev. Nucl. Sci. **8** 49 (1958).

(GC65) A. Gilbert and A. Cameron, Can. J. Phys. **43** 1446 (1965).

(GPT68) W. Greenlees, G. Pyle and Y. Tang, Phys. Rev. **171** 1115 (1968); also Phys Rev. **C1** 1145 (1970).

(Hod63) P. Hodgson, **The Optical Model of Elastic Scattering** Clarendon, Oxford (1963).

(Hod94) P. Hodgson, **The Nucleon Optical Model** World Sci. Pub., Singapore (1994).

(Lan+61) R. Lane et al., Ann. Phys. **12** 135 (1961).

(Lan62) A. Lane, Nucl. Phys. **35** 676 (1962); also Phys. Rev. Lett. **8** 171 (1962).

(LGS87) R. Lawson, P. Guenther and A. Smith, Phys. Rev. **C36** 1298 (1987).

(Lip66) R. Lipperheide, Nucl. Phys. **89** 97 (1966).

(LS01) R. Lawson and A. Smith, Argonne Natl. Lab. Report **ANL/NDM-152** (2001).

(MDH81) S. Mughabghab, M. Divadeenam and N. Holden **Neutron Cross Sections** Academic, New York, (1981); and private communication.

(MN59) B. Mottelson and S. Nilsson, Kgl. Danske Videnskab Selskab. Mat. Fys. Skrifter **1** 8 (1959).

(MN81) C. Mahaux and H. Ngo, Phys. Lett. **100B** 285(1981).

(Mol80) P. Moldauer, Nucl. Phys. **A344** 185 (1980).

(MY87) R. Macklin and P. Young, Nucl. Sci. and Eng. **97** 239 (1987).

(NDS) Nuclear Data Sheets; A. Artuna-Cohen, **79 1 (1996);** C. Reich and R. Helmer **85** 171 (1998); C. Reich, **71** 709 (1994); C. Reich **99** 753 (2003); R. Helmer **78** 219 (1996); R. Helmer **101** 325 (2004); C. Reich **78** 547 (1996).

(NNDC) National Nuclear Data Center, Brookhaven Natl. Lab.

(Pas67) G. Passatore, Nucl. Phys. **A95** 694 (1967).

(PB62) F. Perey and B. Buck, Nucl. Phys. **32** 353 (1962).

(Pre62) M. Preston, **Physics of the Nucleus** Addison-Wesley, Reading, MA (1962).

(Ray96) J. Raynal, The Coupled Channels Code **ECIS96**, private communication, see also CEA Report **CEA-N-2772** (1994).

(Sat69) G. Satchler, **Iso-spin in Nuclear Physics**, Ed. D. Wilkinson, North-Holland, Amsterdam (1969).

(Sat83) G. Satchler, **Direct Nuclear Reactions** Addison-Wesly, Reading, MA (1983).

(Smi90) A. Smith, **Argonne Memorandum** (1990), unpublished.

(Smi92) A. Smith, Argonne Natl. Lab. Report **ANL/NDM-127** (1992); see also Phys.

Rev.**C45** 1260 (1992); Z. Phys. **A360** 265 (1982); Nucl. Instr. and Methods **50** 277 (1977); and references cited therein.

(Smi99) A. Smith, Argonne Natl. Lab. Report **ANL/NDM-147** (1999).

(Smi00) A. Smith, Argonne Natl. Lab. Report **ANL/NDM-151** (2000); also A. Smith, Ann. Nucl. Energy **28** 1745 (2001).

(Smi01) A. Smith, Argonne Natl. Lab. Report **ANL/NDM-153** (2001); also A. Smith, Ann. Nucl. Energy **29** 1241 (2002).

(Smi03) A. Smith, Argonne Natl. Lab. Report **ANL/NDM-155** (2003), also J. Phys. **G30** 407 (2004).

(SSW70) G. Sherwood, A. Smith and J. Whalen, Nucl. Sci. and Eng. **37** 67 (1970).

(Tam65) T. Tamura, Rev. Mod. Phys. **37** 679 (1965).

(Tan72) W. Tanaka et al., **Proc. Budapest Conf.** 148 (1972).

(Tul90) J. Tuli, **Nuclear Wallet Cards,** National Nuclear Data Center, Brookhaven Natl. Lab. (1990).

(WG86) R. Walter and P. Guse, **Proc. of Conf. on Nucl. Data for Basic and Applied Sci.** Eds. P. Young et al., **2** 272, Gordon and Breach, New York (1986).

(Wol51) L. Wolfenstein, Phys. Rev. **82** 690 (1951).

(YA87) P. Young and E. Arthur, Los Alamos Natl. Lab. Report **LA10915-PR,** 31 (1987).

APPENDIXES

Appendix A-1. Total Cross Section Measurements

There have been nine measurements of elemental gadolinium fast-neutron total cross sections, all more than a quarter of a century old, as cited below. There are no experimental results above 20 MeV. The available experimental information was ordered by energy and running averages were constructed over averaging increments of 10 keV below 0.1 Mev, over 50 keV from 0.1-0.5 Mev, over 0.1 Mev from 0.5-5.0 Mev and over 0.2 Mev at higher energies. These averaged measured total cross sections are illustrated in a number of the present figures (e.g. see **Figure III-A-1**). They give a reasonable description of the total cross sections up to nearly 20 Mev, and extend over the entire energy range of the measured differential-scattering cross sections.

1. G. Sherwood, A. Smith and J. Whalen, Nucl. Sci. and Eng. **39** 67 (1970).
2. J. Conner., Phys. Rev. **109** 1268 (1958).
3. K. Seth. et al., Phys. Lett. **16** 306 (1965).
4. J. Kellie et al., J. Phys. **A7** 1758 (1974).
5. M. Husssain et al., J. Nucl. Energy **23** 113 (1969).
6. G. Wickstrom et al., Nucl. Sci. and Eng. **25** 291 (1966).
7. W. Stupega et al., private communication to NNDC (1966).
8. M. Hussain., E. Islam and N. Ameen., Nucl. Sci. and Appl. **4** 3 (1968).

9. D. Foster Jr. and D. Glasgow, Phys. Rev. **C3** 576 (1971).

Appendix A-2. Prior Elastic-Scattering Measurements

Prior knowledge of "elastic" neutron scattering from elemental gadolinium is limited to three measurements, all more than a quarter of a century old, as cited below. The first of these is a single, approximately 1 Mev, scattering distribution by Gilboy and Towle . The second set is the result of a comprehensive study by Sherwood et al. with 65 distributions distributed over the incident neutron energy range 0.3 -1.5 Mev. This is the early work at this laboratory discussed in the body of the text. The third set consists of six elastic distributions distributed between 1.5 and 3.6 Mev by Tanaka et al. There was no other elemental gadolinium elastic-scattering information prior to the present measurements

1. W. Gilboy and J. Towle, Nucl. Phys. **42** 86 (1963).
2. G. Sherwood, A. Smith. and J. Whalen, Nucl. Sci. and Eng. **39** 67 (1970).
3. S. Tanaka et al., Proc. Budapest Conf. 148 (1972).

Appendix A-3. Prior Inelastic Scattering Measurements

There are six citations in CINDA to measurements of inelastic neutron scattering from gadolinium and/or its isotopes relevant to the present work, as listed below. Half of them report results of elemental or isotopic (n,n';gamma) measurements from which neutron inelastic-scattering cross sections were construed. Sherwood el al. reported detailed measurements of elemental neutron inelastic scattering up to incident energies of 1.5. They compliment and extend the present work, as discussed in the body of the text. Owens and Towle reported inelastic-neutron evaporation spectra at an incident energy of approximately 1.0 MeV using elemental samples. Tanaka et al. reported five elemental inelastic distributions at incident energies in the range of approximately 1.5 - 3.6 Mev. The results construed from (n;n',gamma) measurements are largely relevant to isotopic targets (references 4-6, below).

1. G. Sherwood, A. Smith. and J. Whalen, Nucl. Sci. and Eng. **39** 67 (1970).
2..R. Owens. and J. Towle, Nucl. Phys. **A112** 337 (1968).
3. W. Tanaka et al., Proc. Budapest Conf., 148 (1972).
4. E. Konobeevskij. et al., Proc. Kiev Conf. **3** 203 (1983).
5. Y. Efrosinin et al., Proc. Riga Conf. 274 (1979).
6. S. Elbakr et al., Phys. Rev. **C10** 1864 (1974).

TABLES

Table III-A-1.. SOM parameters resulting from the fitting procedures described in the text. Potential depths of V and W are given in units of MeV. Strengths J_i are expressed as volume-integrals-per-nucleon in units of MeV-fm^3. Geometrical dimensions are given in fms. V, W and J_i are "scalar" values, as defined in the text. Throughout this work potential parameters are given to sufficient precision to permit accurate reproduction of the calculated results. That precision does not necessarily imply uncertainty.

Real Potential

Strength

$V = 45.578 - 0.1337 \cdot E$

$J_V = 381.13 + 1.118 \cdot E$

Reduced Radius

$r_V = 1.2260$

Diffuseness

$a_V = 0.609$

Imaginary Potential

Strength

$W = 14.937 + 2.150 \cdot E$

$J_W = 69.66 + 10.025 \cdot E$

Reduced Radius

$r_W = 1.4137$

Diffuseness

$a_W = 0.250$

Spin-Orbit Potential (**WG86**)

Strength

$V_{so} = 6.147 - 0.015 \cdot E$

Reduced Radius

$r_{so} = 1.1030$

Diffuseness

$a_{so} = 0.560$

Table III-A-2. SOM parameters obtained with the isotopic approximation described in the text. The nomenclature is the same as that of **Table III A-1**, except that the full potential strengths are given rather than the iso-scalar components.

Real Potential

Strength

$V = 44.258 + 0.1818 \cdot E$

$J_V = 337.98 + 1.388 \cdot E$

Reduced Radius

$r_V = 1.1827$

Diffuseness

$a_V = 0.650$

Imaginary Potential

Strength

$W = 13.545 + 2.157 \cdot E$

$J_W = 60.67 + 9.663 \cdot E$

Reduced Radius

$r_W = 1.4156$

Diffuseness

$a_W = 0.248$

Spin-Orbit Potential (same as **Table A-III-1**)

Table III-B-1. ROTM parameters following from the fitting procedures discussed in the text. The nomenclature is the same as that of **Table III-A-2,** with the addition of deformation parameters. Full potential strengths are given.

Real Potential

Strength

$V = 46.418 - 0.085 \cdot E$

$J_V = 435.38 - 0.797 \cdot E$

Reduced Radius

$r_V = 1.245$*

Diffuseness

$a_V = 0.650$*

Imaginary Potential

Strength

$W = 3.500 + 0.332 \cdot E$

$J_W = 25.87 + 2.4525 \cdot E$

Reduced Radius

$r_W = 1.245$*

Diffuseness

$a_W = 0.500$*

Spin-Orbit Potential (same as **Table III-A-1**)

Deformation

$\beta_2 = 0.308$

$\beta_4 = 0.056$

* Geometries taken from reference **YA87.**

Table III-C-1. Parameters of the ROTM dispersion potential deduced as described in the text. The nomenclature is identical to that of **Table III-B-1**.

Real Potential

Strength

$V = 43.948 - 0.1158 \cdot E$

$J_V = 411.26 - 1.0837 \cdot E$

Reduced Radius

$r_V = 1.245$*

Diffuseness

$a_V = 0.650$*

Imaginary Potential

Strength

$W = 3.4841 + 0.2992$

$J_W = 25.74 + 2.2104 \cdot E$

Reduced Radius

$r_W = 1.245$*

Diffuseness

$a_W = 0.500$*

Spin-Orbit Potential (same as **Table III-A-1**)

Deformations (same as **Table III-B-1**)

* Geometries taken from reference **YA87.**

Table IV-1 (A). Full regional-potential strengths given as volume integrals per nucleon, J_i, in units of Mev-fm^3. Other symbols and dimensions are defined in the text. Average mass = 168.4 AMU..

Target	Z	A	η	β_2	Ji	Reference
Hf	72	178.5	0.191	0.287	$J_V = 457.15 - 2.593 \cdot E$ $J_W = 19.5 + 2.419 \cdot E$	**Smi01**
Ho	67	164.9	0.188	0.300	$J_V = 444.39 - 3.558 \cdot E$ $J_W = 22.4 + 2.151 \cdot E$	**Smi00**
Re	75	186.2	0.194	0.220	$J_V = 428.94 - 3.189 \cdot E$ $J_W = 18.3 + 2.258 \cdot E$	**Smi03**
Gd	64	157.3	0.186	0.300	$J_V = 434.44 - 0.796 \cdot E$ $J_W = 25.9 + 2.453 \cdot E$	This work
Gd	64	157.3	0.186	0.300	$J_V = 434.81 - 2.059 \cdot E$ $J_w = 17.4 + 2.708 \cdot E$	**YA87**
Ho	67	164.9	0.188	0.300	$J_V = 449.97 - 3.125 \cdot E$ $J_W = 25.5 + 2.363 \cdot E$	**YA87**
Eu	63	152.0	0.171	0.160	$J_V = 455.95 - 3.147 \cdot E$ $J_W = 20.0 + 3.846 \cdot E$	**YA87**
Re	75	186.2	0.194	0.220	$J_V = 432.71 - 2.780 \cdot E$ $J_W = 16.5 + 4.931 \cdot E$	**MY87**

Table IV-1 (B). Regional average potential parameters. Full potential strengths are given.

Real potential

$J_V = 442.28 - 3.045 \cdot E$

$V = 46.382 - 0.3193 \cdot E$

$r_V = 1.2568$

$a_V = 0.6292$

Imaginary potential*

$J_W = 20.7 + 2.891 \cdot E$

$W = 2.911 + 0.410 \cdot E$

$r_W = 1.2629$

$a_W = 0.4785$

* Linear approximation extending to 10 Mev or the onset of volume absorption, whichever is lower in energy.

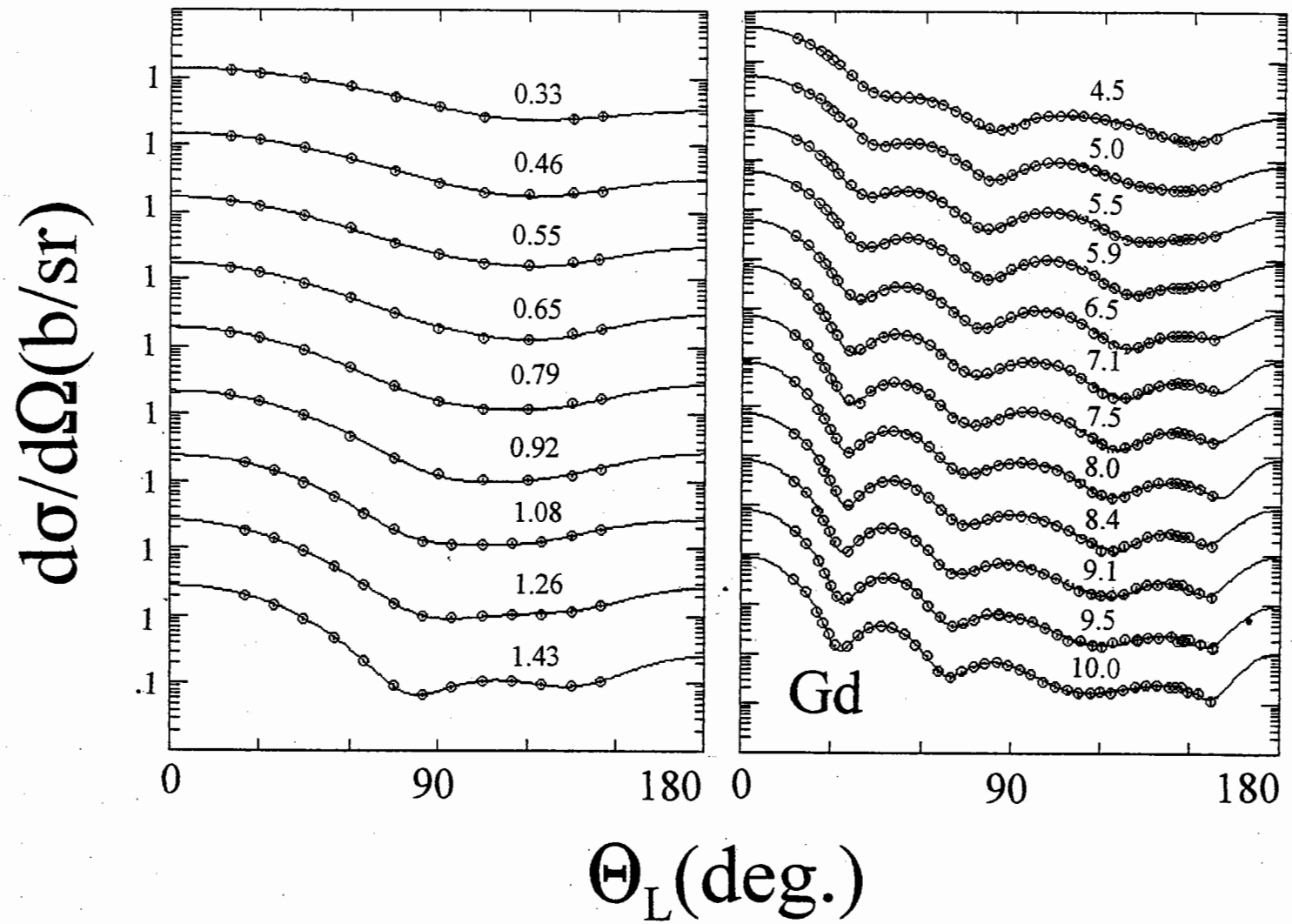

Figure II-1. Measured differential "elastic"-scattering cross sections of elemental gadolinium. The present measured values are indicated by symbols, curves denote the results of fitting the measured results with legendre-polynomial expansions. Approximate incident-neutron energies are numerically noted in MeV. Throughout this work data is presented in the laboratory coordinate system.

Figure. III-A-1. Measured (symbols) and calculated (curves) neutron total cross sections of elemental gadolinium. The symbols follow from averages of the measured total-cross-section data as described in Appendix **A-1**. The upper panel was obtained using the elemental SOM of **Table III-A-1** and the lower panel using the ^{158}Gd SOM approximation of **Table III-A-2**.

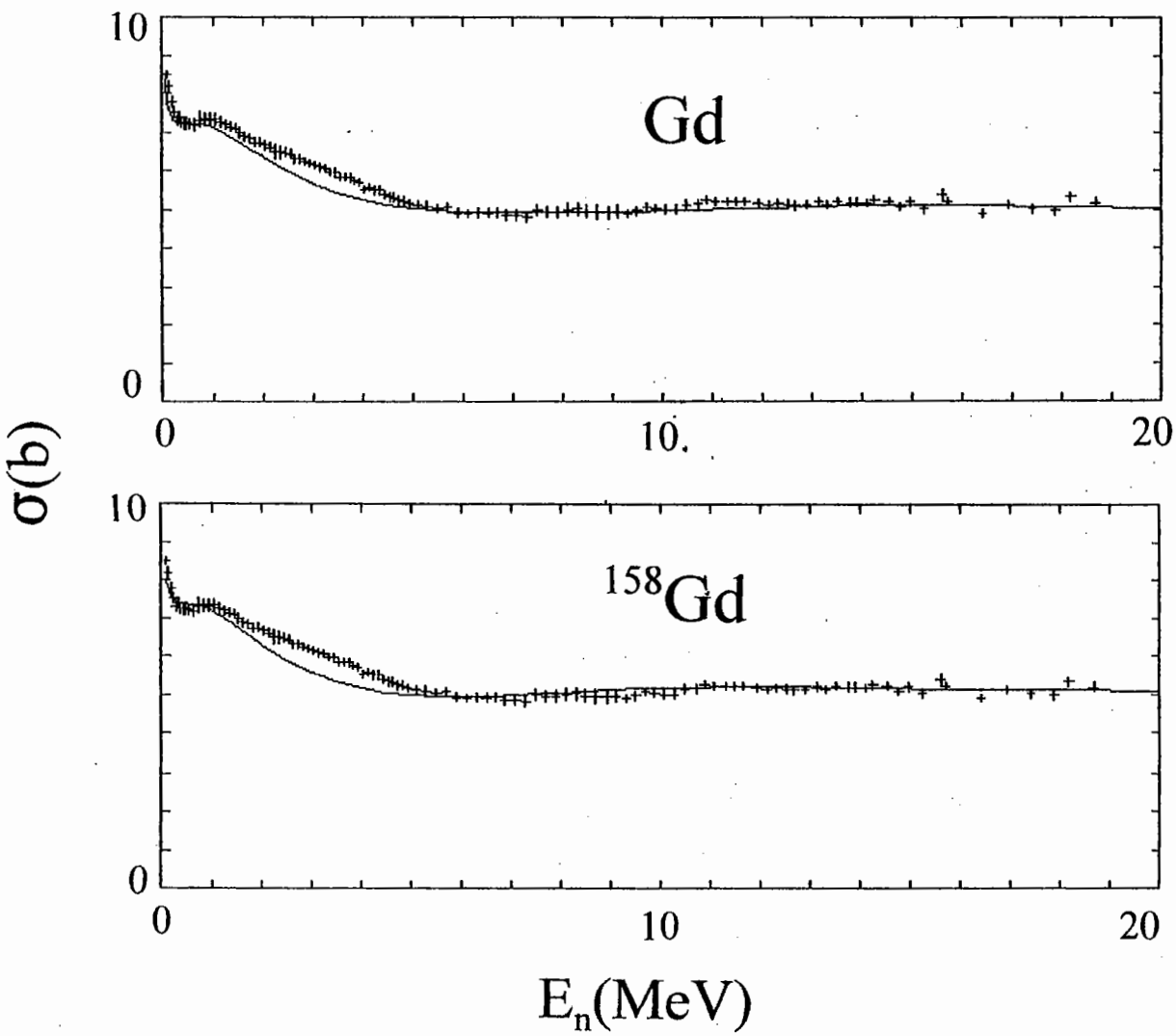

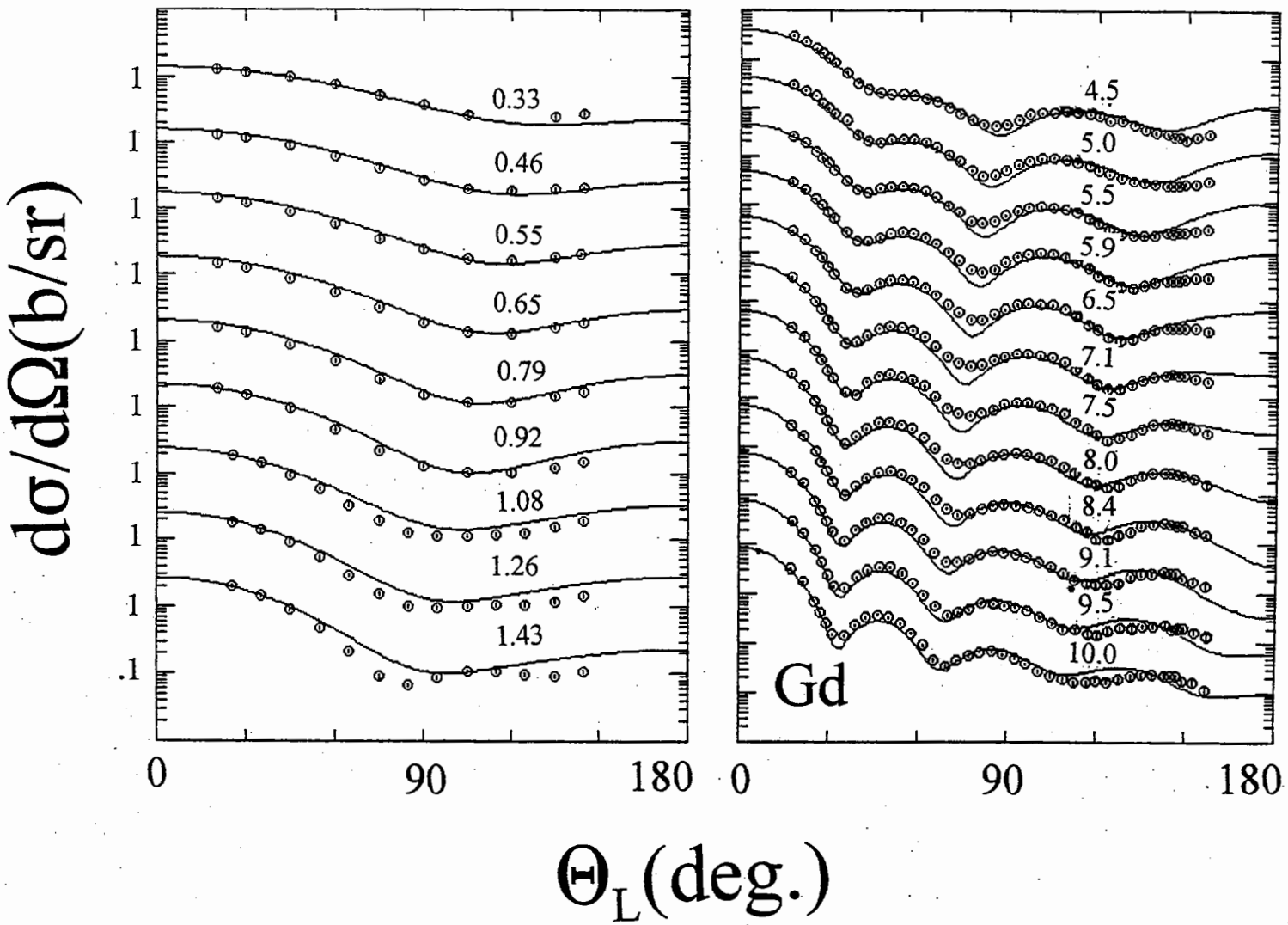

Figure. III-A-2. Comparison of measured and SOM-calculated differential "elastic"-neutron scattering from elemental gadolinium. Symbols indicate the present measured values, curves the results of calculations using the SOM potential of **Table III-A-1**. Approximate incident-neutron energies are numerically given in Mev.

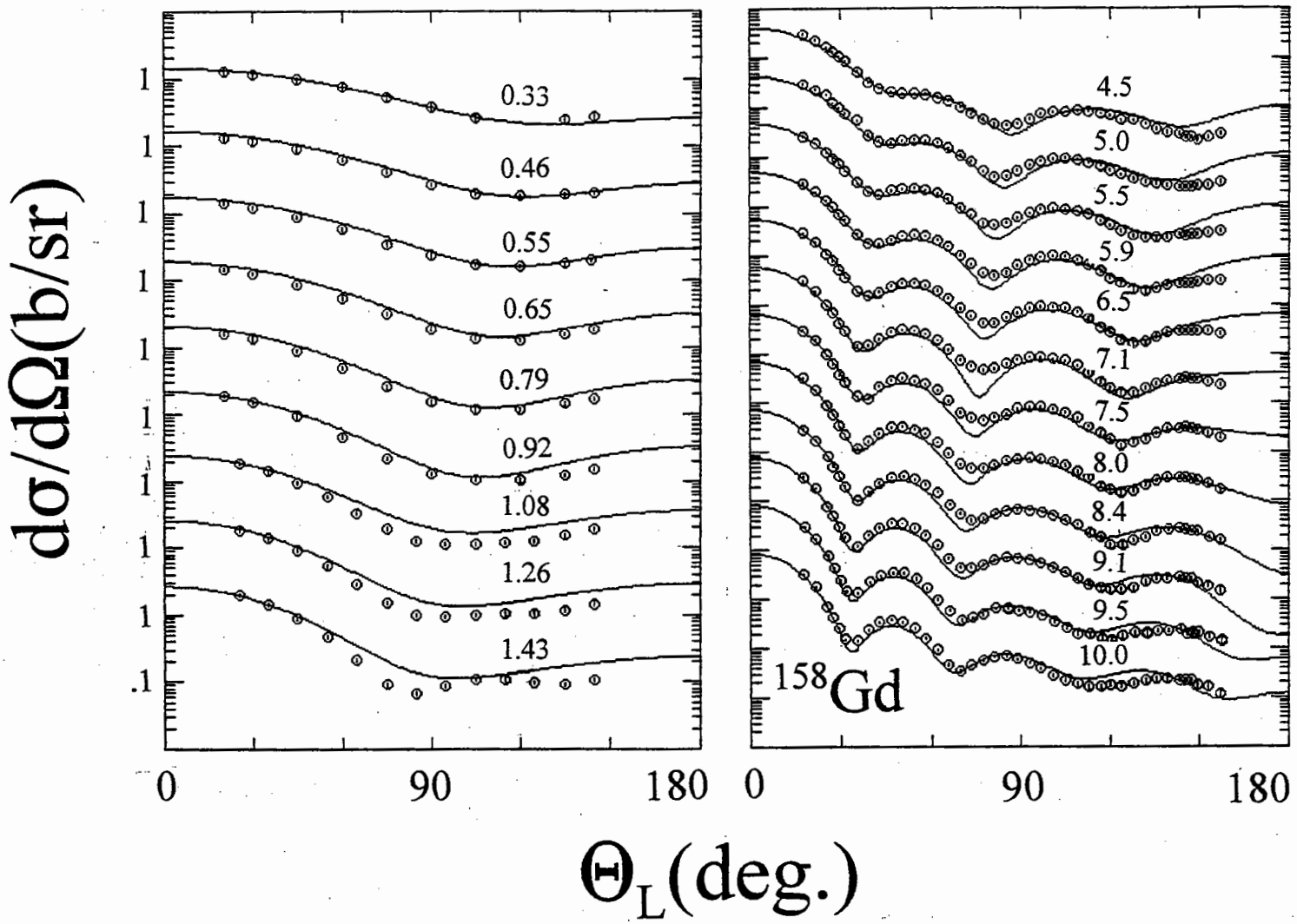

Figure III-A-3. Comparison of measured and calculated differential "elastic"-neutron scattering from elemental gadolinium. The calculations use the isotopic approximation and parameters of **Table III-A-2,** as described in the text. The nomenclature is identical to that of **Fig. III-A-2**.

Figure III-B-1. Comparison of measured and calculated neutron total cross sections of elemental gadolinium. Symbols indicate the energy-averaged experimental values as described in Appendix **A-1**. The curve is the result of calculations using the ROTM potential of **Table III-B-1**.

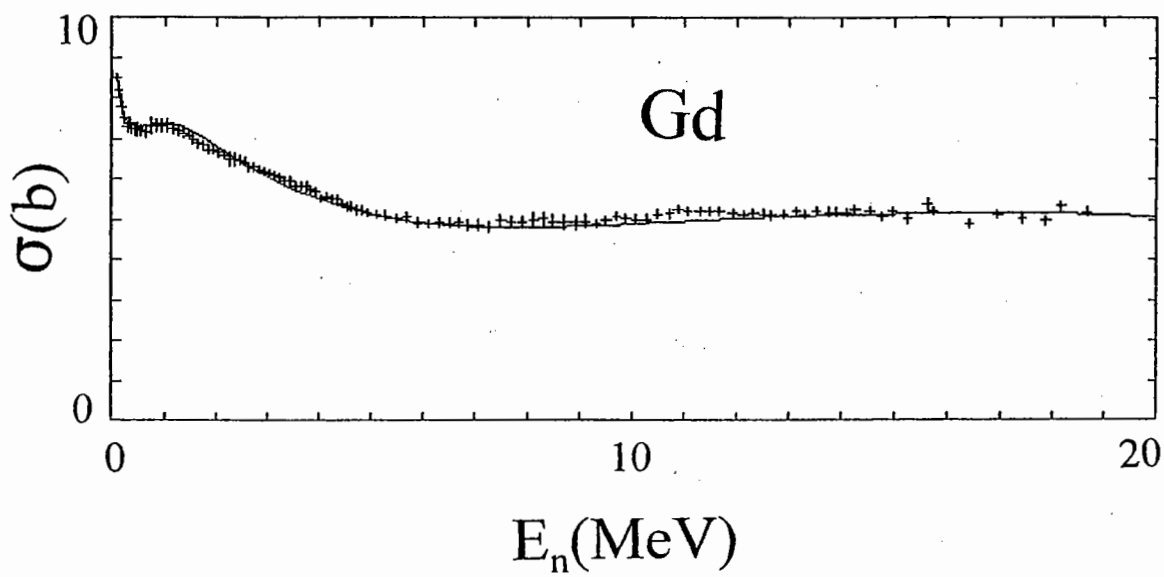

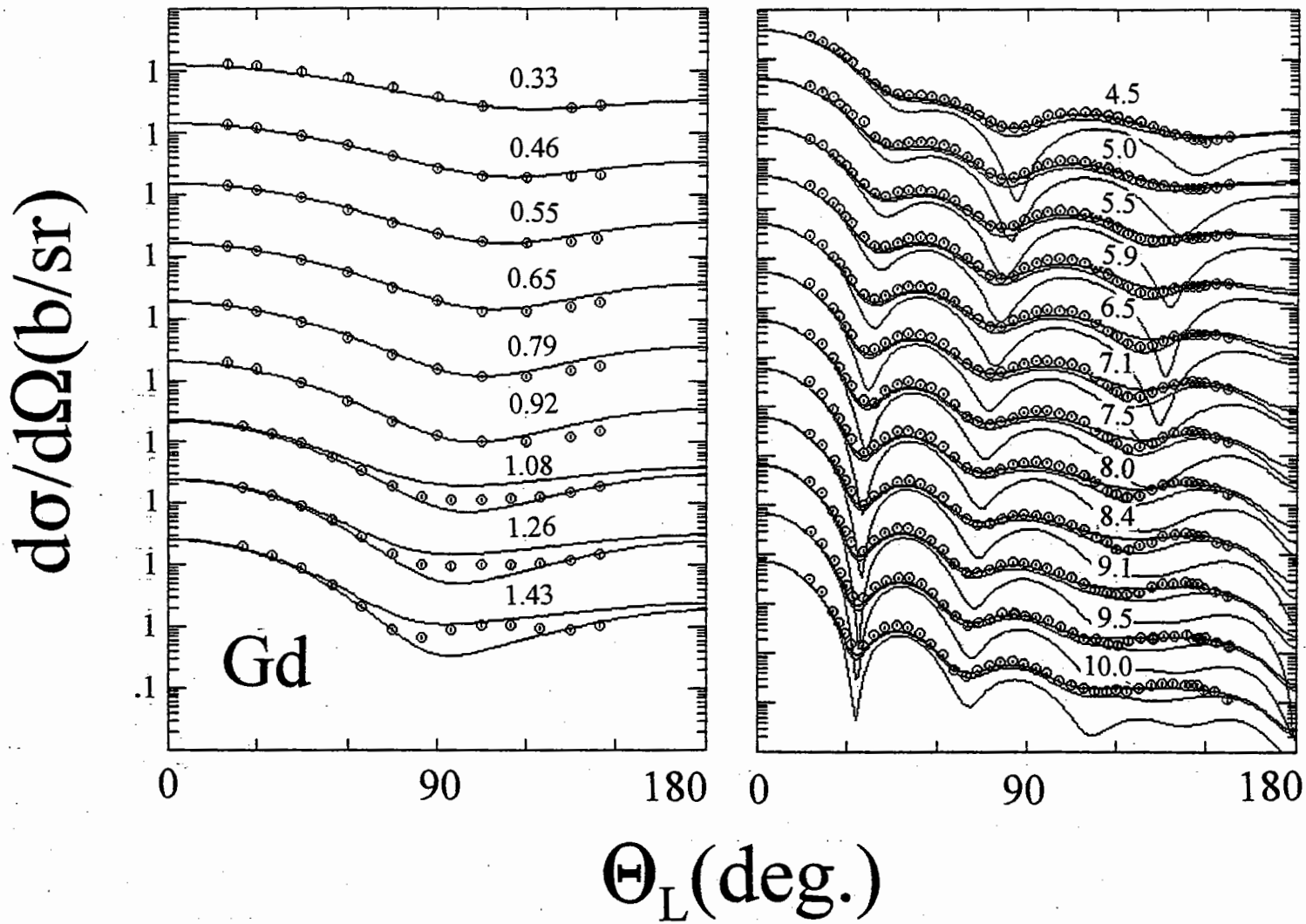

Figure. III-B-2. Comparisons of measured and calculated neutron differential "elastic" scattering cross sections of elemental gadolinium. The measured values are indicated by symbols and ROTM-calculated results by curves. Approximate incident-neutron energies are numerically noted. Where there is one curve at a given energy it represents the calculated elastic-scattering component. Two curves at a given energy indicate the elastic and the elastic+first inelastic contributions. Three curves at an energy indicate elastic, elastic+first inelastic, and the elastic+first inelastic+second inelastic contributions, as discussed in the text.

Figure III-B-3. Measured and calculated inelastic-scattering cross sections resulting from the excitation of the first two excited levels of the postulated g.s. rotational band (E_x= 0.08 MeV and = 0.26 MeV), as described in the text. Circular symbols indicate experimental results of the present work and that of reference **SSW70**, and crosses the measured values reported in reference **Tan+72**. Curves indicate the results of ROTM calculations as described in the text.

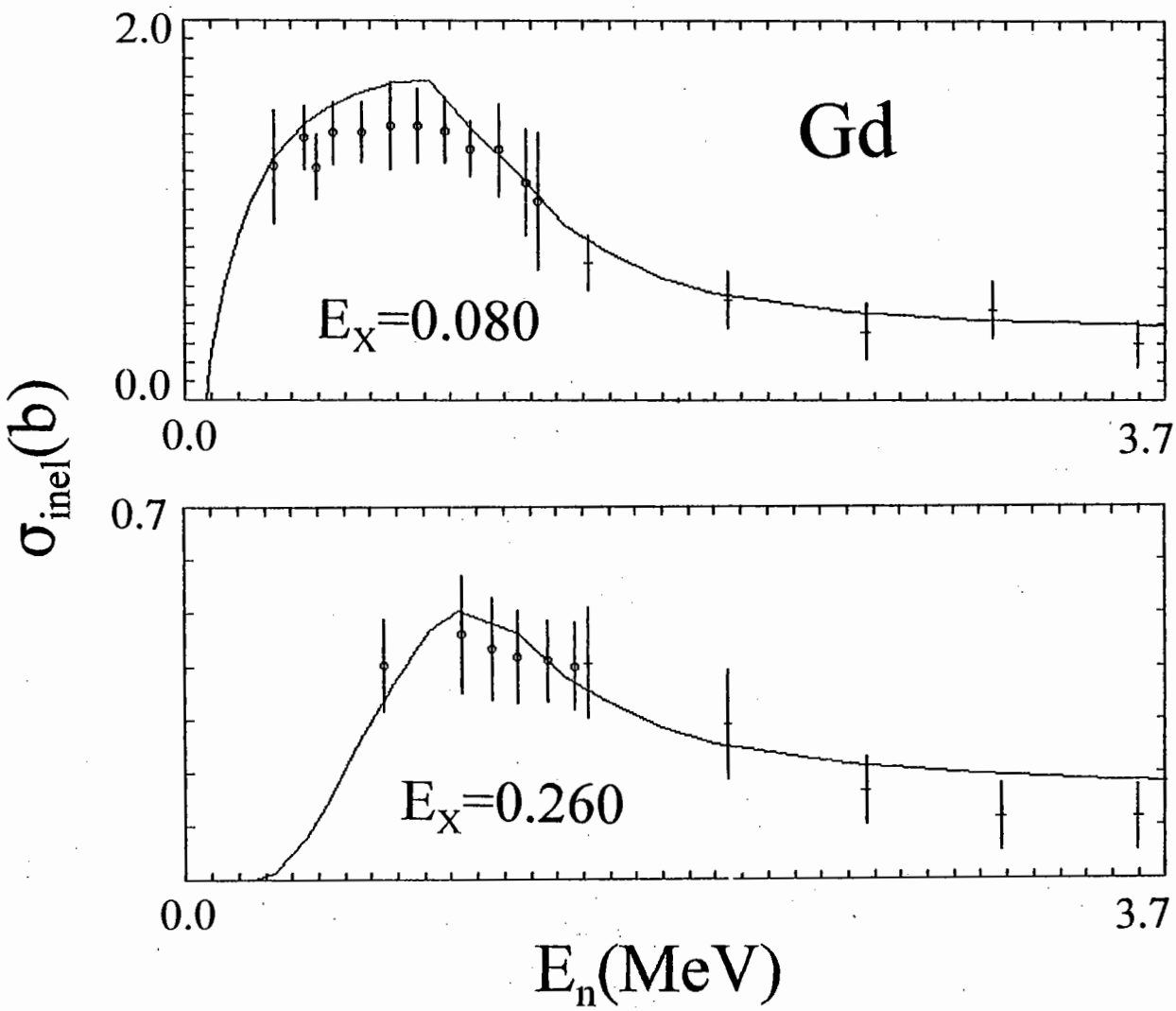

Figure III-C-1. Comparisons of measured and calculated neutron total cross sections of elemental gadolinium. The upper panel compares measured (symbols) and calculated (curve) cross sections where the calculations used the ROTM potential of **Table III-B-1.** The lower panel is a similar representation except that the calculations employed the dispersion ROTM potential of **Table III-C-1**.

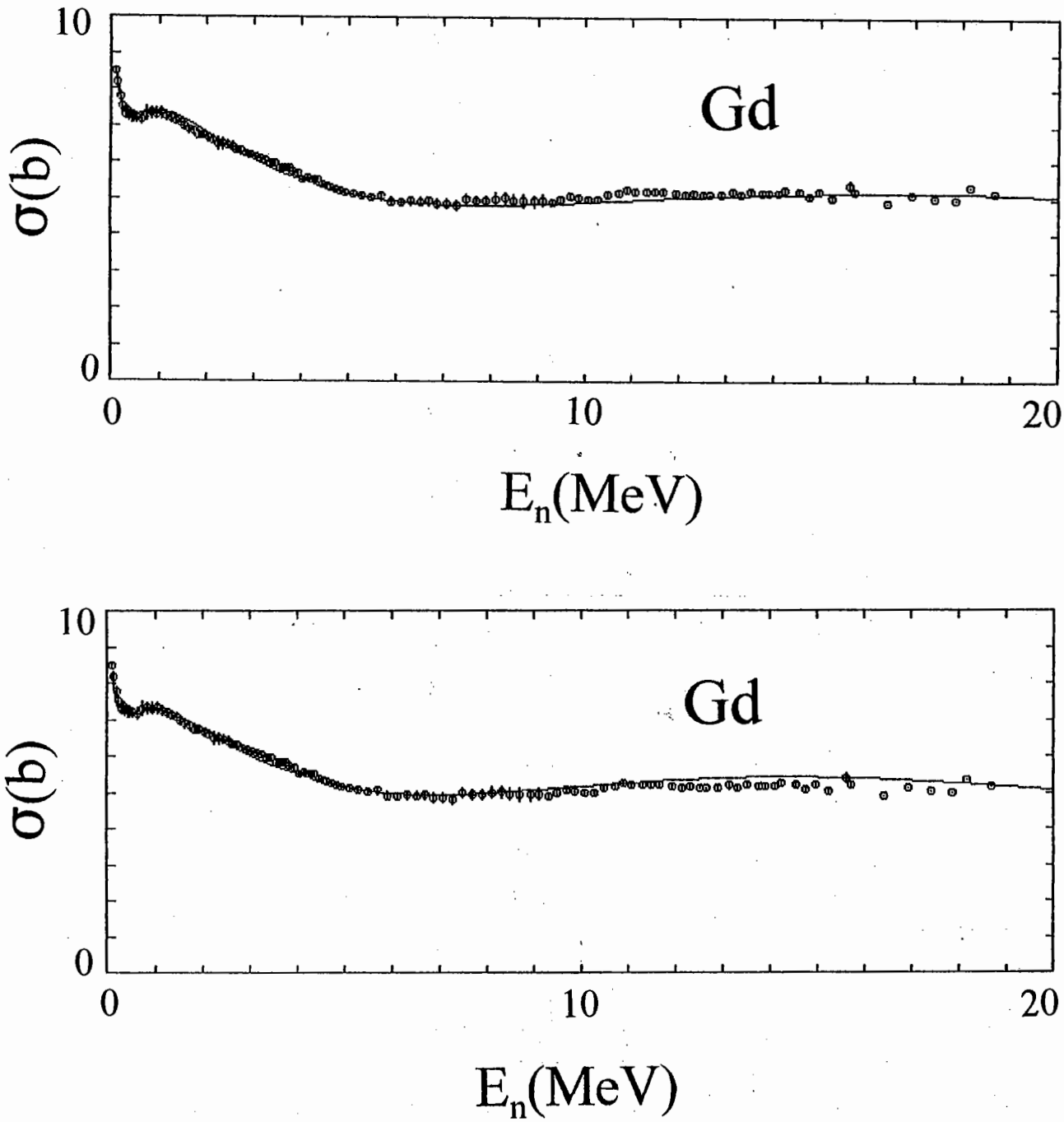

Figure IV-1. Comparison of measured elemental neutron total cross sections of gadolinium (symbols) with the values predicted by the ENDF/B-VI evaluated isotopic files (curve).

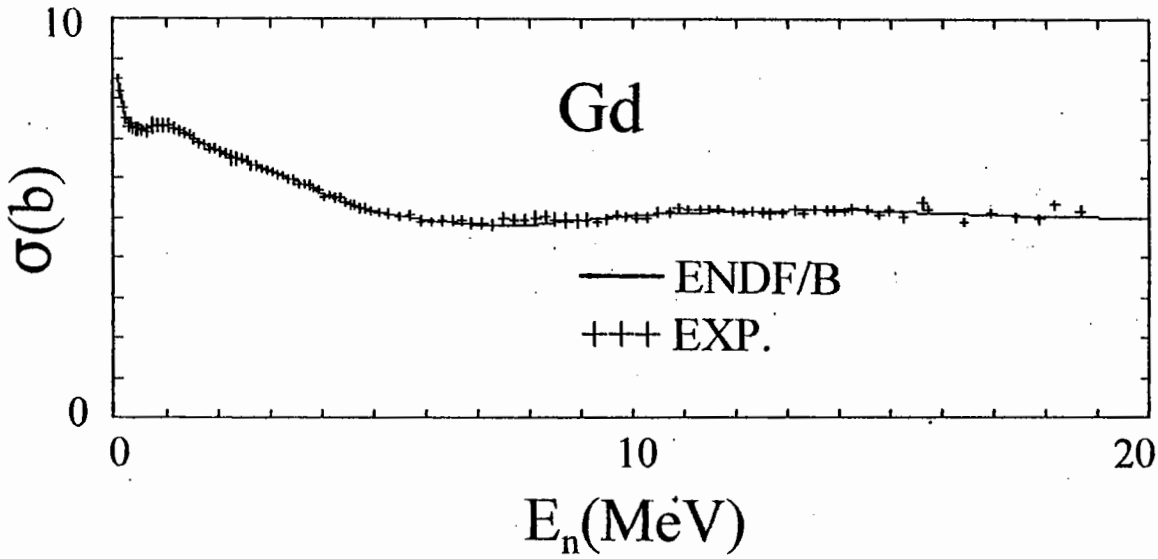

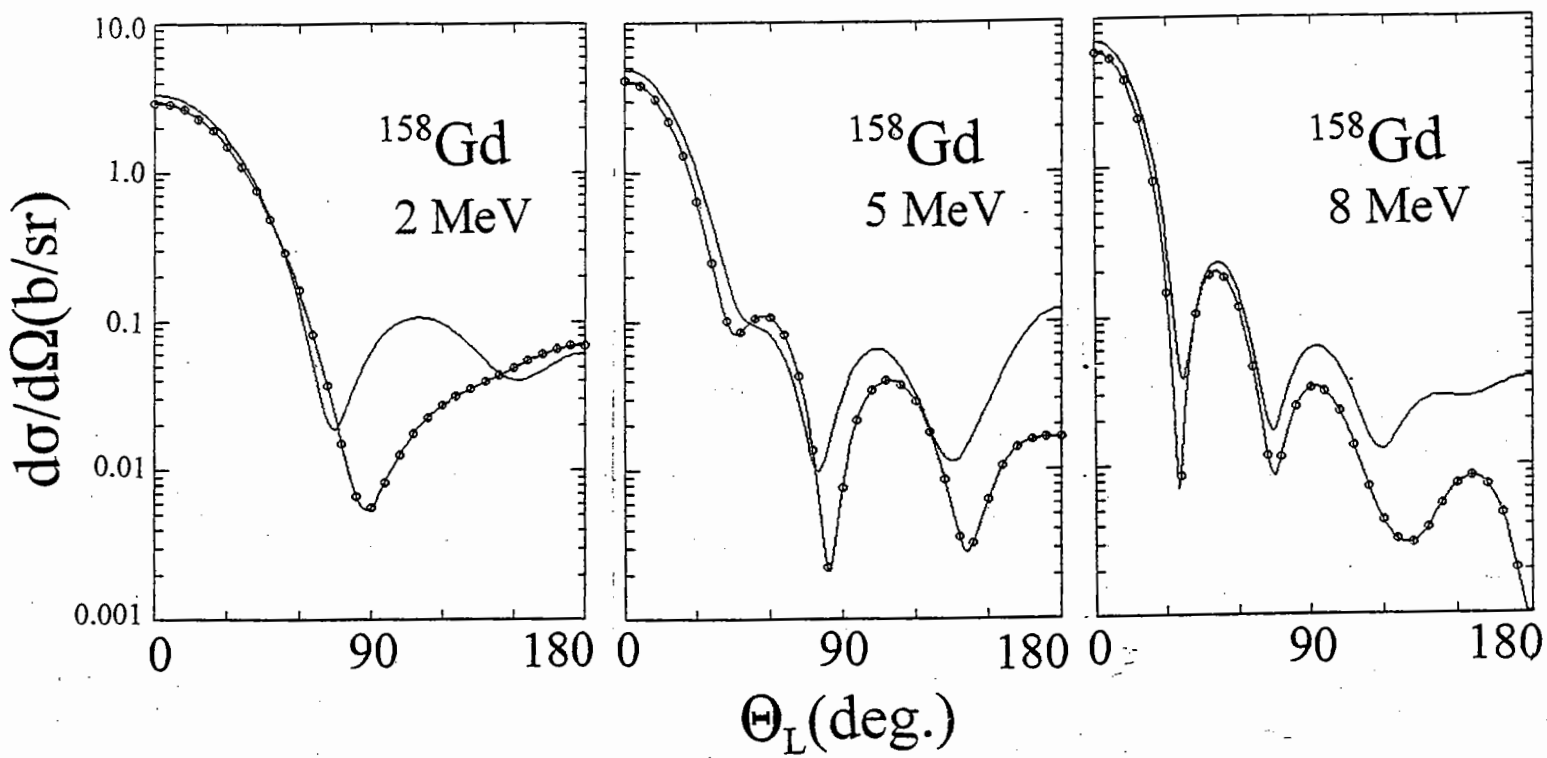

Figure IV-2. Illustrative comparison of ENDF/B-VI evaluated ^{158}Gd differential neutron elastic-scattering cross sections (simple curve) with the results of calculations based upon the ROTM dispersion model of **Table III-B-2** (curve with symbols) at representative incident-neutron energies.

Figure IV-3. Comparison of ENDF/B-VI angle-integrated elastic-scattering cross sections of ^{158}Gd (symbols) with total-elastic, compound-elastic (CE) and direct-elastic (DIR) contributions calculated with the dispersion ROTM (curves as indicated).

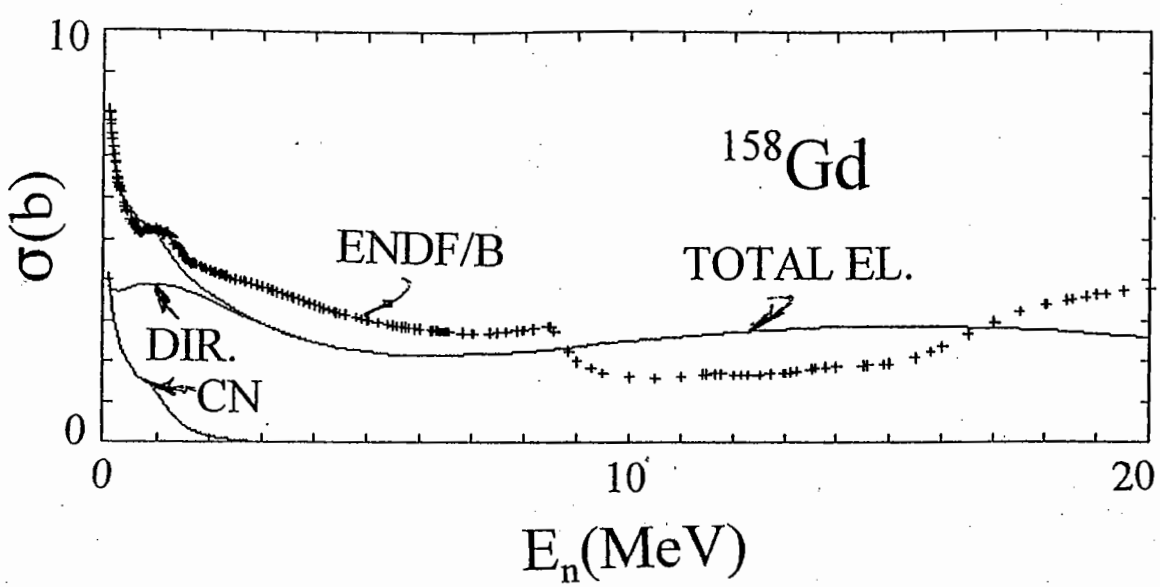
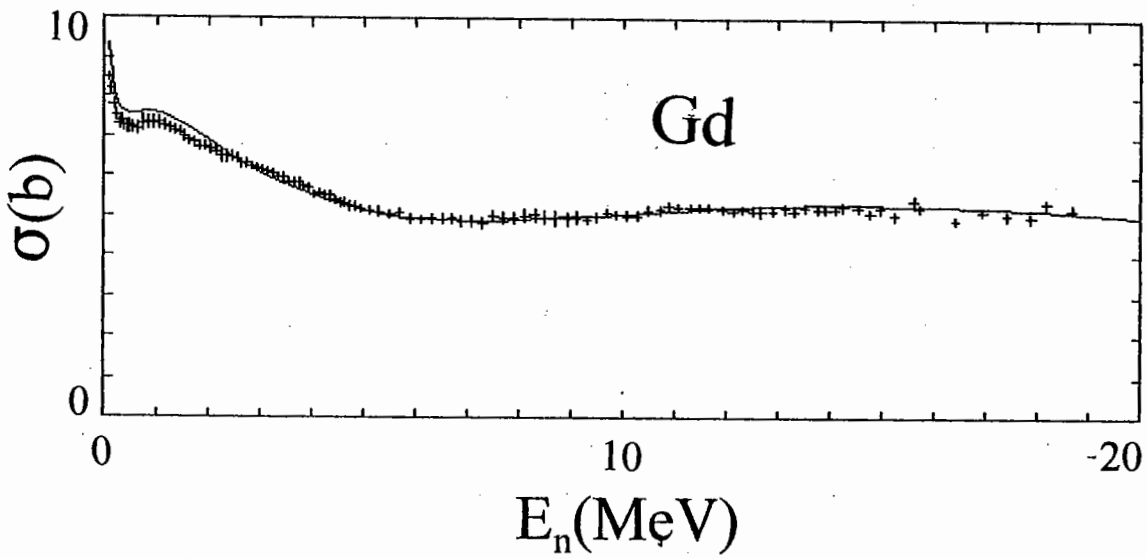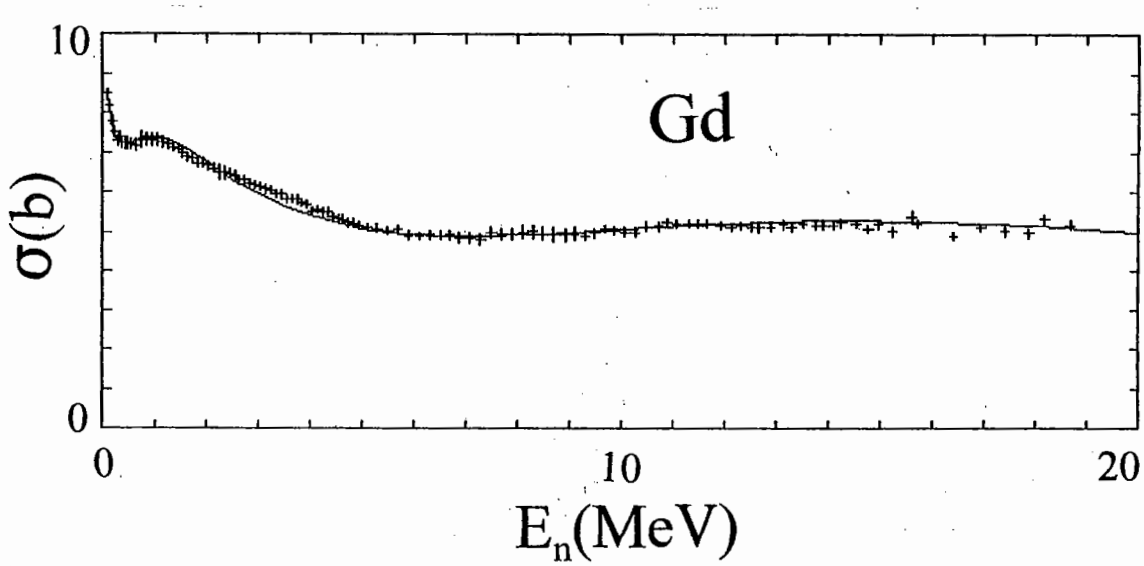
Figure IV-4. Comparison of measured (symbols) and calculated (curves) neutron total cross sections of elemental gadolinium. The upper panel of the figure used the generalized potential of **Table IV(B)** in the calculations. The lower panel of the figure used the generalized potential reduced by 1.0% at zero energy in a linear manner as described in the text.